EAI Endorsed Transactions
on Sustainable Manufacturing and Renewable Energy Research Article EAI.EU

Study on the Assessment of Absorbed Energy of Bulbous Bow in Ship Collision

Quyen Tran-manh[1,2], Hai Tran[1,2*], Tao Tran-van[1,2]

[1]Department of Naval Architecture & Marine Engineering, Faculty of Transportation Engineering, Ho Chi Minh City University of Technology (HCMUT), 268 Ly Thuong Kiet, Dien Hong Ward, Ho Chi Minh City, Viet Nam
[2]Vietnam National University Ho Chi Minh City, Linh Trung Ward, Thu Duc City, Ho Chi Minh City, Vietnam

Abstract

The evaluation of energy absorption characteristics of the bulbous bow structure in ship collisions or grounding accidents is a crucial research area. Predicting dynamic reactions or determining the collision energy absorption capability of the bulbous bow structure during impacts is essential in the design process. This paper investigates the collision behavior of the bulbous bow structure impacting a rigid wall using numerical simulations conducted with the commercial finite element code FEA. Namely, impact force histories on the bulbous bow structure, crushing depths/displacements, and collision energy absorption of the ship structure during impact are numerically determined under, consideration of different collision velocities, ship masses, impact angles and impact positions. The FEM results will be compared to results obtained from AASHTO. The results indicate that collision forces, deformations of the bulbous bow structure, and absorbed collision energies can be effectively predicted using current numerical simulation. The maximum collision force and energy absorption are directly influenced by the collision velocity and mass of the impacting ship. Notably, variations in collision positions (H) and impact angles (α) result in differences in collision forces and deformations at the bulbous bow structure. Therefore, careful consideration of parameters (H) and (α) is crucial to predict structural damage effectively. In addition, the pre-and post-collision motion behavior of the ship is also evaluated using a 6-degree-of-freedom (6 DOF) system.

Keywords: Ship Collision, Impact Dynamics, Energy Absorbed, Bulbous Bow, FEM

Received on 15 July 2025, accepted on 13 September 2025, published on 23 September 2025

doi: 10.4108/eetsmre.9723

*corresponding author. Email: haitran@hcmut.edu.vn

1. Introduction

Maritime traffic accidents pose significant potential consequences, greatly affecting human lives and resulting in substantial material damage. Research on the assessment of collision impacts and structural damage, ranging from minor structural impairments to severe threats to a ship's structural integrity, remains a critical topic.

1.1. General context

According to Yu and Amdalh [1], to design safer and more cost-effective ships and offshore structures capable of withstanding random loads, it is necessary to consider the influence of external dynamics, in addition to the internal mechanical impacts that were the focus of previous studies [2][3][4].

In recent years, evaluating the energy absorption capacity of the ship's bow in collisions has remained a topic of great interest [5][6][7]. The objective of this paper is to employ the finite element method (FEM) to develop collision models, analyse forces, energy dissipation, and assess the factors influencing damage resulting from collisions. The analysis results will provide data to aid in the structural design of maritime vessels, predicting collision resistance and gaining insights into the impact-resistance characteristics of structures. This information will enhance ship design by considering impact loads, rather than solely focusing on static loads as in traditional approaches. The absorption of collision energy by structures is also a key issue discussed in this study.

1.2. Research novelty

In recent decades, Minorsky was the first to lay the foundation for ship collision analysis, and his method has been still widely used and referenced today. Based on an investigation of 26 ship-to-ship collision cases, Minorsky [8] proposed a relationship between the mass of the damaged steel structure and the energy absorbed during the collision. Minorsky's method is based on the conservation of momentum and assumes that the collision is completely inelastic. Additionally, the motion is constrained to one dimension, which makes the construction of the analytical model feasible. The linear correlation between the mass of the damaged steel structure and the absorbed energy is defined as

$$E_T = 414.5 \times R_T + 121.900, \quad (1)$$

where E_T(tons-knots^2) is the energy absorbed during collision, and R_T(ft^{2}in) is the resistance coefficient or the mass of the damaged steel structure.

Minorsky proposed that the total absorbed energy (as well known as lost kinetic energy in MJ) is

$$\Delta KE = \frac{M_B \times M_A}{1.43M_B + 2M_A} \times [v_B \sin(\emptyset)]^2, \quad (2)$$

with the masses of the colliding ships denoted as M_B and M_A, respectively, and the initial velocity of the colliding ship as v_B. The equation (3) is provided to calculate the impact angle of 90 degrees

$$\Delta KE = \frac{M_B \times 1.4M_A}{2(M_B + 1.4M_A)} \times v_B^2. \quad (3)$$

It should be noted that equations (2) and (3) take into account the roll motion of the struck ship in the direction the ship is moving at the moment of impact. This increases the mass of the struck ship due to the involvement of the hydrodynamic mass of the surrounding water.

By plotting the absorbed kinetic energy in the damaged ship structures during collisions against the volume of damaged steel material in several collision cases, as reported by Minorsky, and fitting the data points using the linear least squares method, the correlation between kinetic energy and the damaged mass is calculated according to the following equation

$$\Delta KE = 47.2 \times R_T + 32.7. \quad (4)$$

This approach has been widely adopted and modified by numerous other researchers. Reardon and Sprung [9] re-evaluated Minorsky's correlation by incorporating new collision cases beyond Minorsky's original 1959 data and estimated from seven additional collisions. Minorsky's assumptions did not account for the energy from the motion of the struck ship, considering only a 40% increase in the mass of the struck ship due to roll motion. Paik, Choe, and Thayamballi [10] discarded Minorsky's first assumption and argued that the kinetic energy generated in a collision is a function of the relative velocity between the two ships.

1.3. Ship motion

In most previous studies, the motion of any ship is considered as a rigid floating body, which can be described using six degrees of freedom (6DOF) system (surge, sway, heave, pitch, roll, yaw). However, similar to maneuvering, a ship involved in a collision can be described using only three degrees of freedom (3DOF) (surge, sway, yaw), where the heave, pitch, and roll movements can be neglected because the energy transferred to these degrees of freedom is minimal compared to the surge, sway, and yaw movements.

In recent decades, a common approach has been to separate the problem into two parts: external dynamics and internal mechanics. The external dynamics model simplifies the effects of the fluid as a constant added mass, so that the entire collision system is unaffected, and applies the principle of conservation of momentum. This allows for a quick estimation of energy dissipation with reasonable accuracy. Pedersen and Zhang [11] proposed a closed-form theoretical model for the flat external dynamics problem. Stronge [12] developed an advanced solution for three-dimensional (3D) impacts. Liu and Amdahl [13] extended Stronge's work to 3D collision cases in a local coordinate system, allowing for the consideration of contact geometric shapes and objects with 3D eccentricity, such as drifting icebergs. When the velocities of the attacking and impacted ships before and after the collision are known, the energy loss in the collision can be obtained with external dynamics models. This lost energy is dissipated through structural deformations in the internal mechanic's assessment, where the attacked ship is typically fixed in space and the attacking ship follows a prescribed path. The final penetration is obtained when the area under the force penetration curve equals the energy loss from the external dynamic calculations.

The separated approach provides a quick and reasonable estimate of energy dissipation and structural damage. However, it has clear limitations in several aspects. First, the effect of the fluid is significantly simplified. Motora et al. [14] found that the assumption of a constant added mass is often not a good approximation. They demonstrated both experimentally and analytically that the equivalent added mass depends on the collision duration and the time variation of the collision force. Collisions with longer durations will result in greater equivalent added mass. These effects are not accounted for in the separate approach. Additionally, the ship's path is prescribed in the internal mechanics assessment, thus neglecting the impact of global ship motion. For asymmetric ship collisions, the separated approach does not predict the exact penetration path accurately, and the error can be significant as shown by Tabri [15] and Yu and Amdahl [16], where the structural damage is found to be quite different from the combined solution.

1.4. AASHTO Guidelines

The American Association of State Highway and Transportation Officials (AASHTO) is a non-profit professional organization that represents transportation agencies from states, counties, and other governmental bodies in the United States. AASHTO is responsible for

developing technical standards and guidelines related to the design, construction, maintenance, and operation of transportation systems, including roads, bridges, and other related infrastructure.

In the AASHTO LRFD Bridge Design Specifications [17], specific provisions are outlined regarding impact loads from vehicles, including ships, on bridges and related structures. These standards aim to ensure that bridges and related structures can withstand collisions from vessels, maintaining safety and stability. The kinetic energy of a moving ship absorbed during a non-eccentric collision with a bridge pier, according to AASHTO guidelines, is calculated as follows

$$KE = \frac{C_H \times W \times V^2}{29.2}, \quad (5)$$

where KE is the ship's impact energy (kip-ft); W is the total displacement of the ship (tons); C_H is the hydrodynamic mass coefficient; and V is the ship's impact velocity (ft/s).

The displacement weight of the ship-W must be based on the ship's loading condition and should include the ship's lightweight, along with considering the cargo weight-DWT (Deadweight Tonnage) for loaded vessels, or ballast weight for ships in transit in light or unloaded condition. The displacement weight of a tug-barge system should be the total displacement of the tug/towboat and the total displacement of a string of barges along the length of the tow.

AASHTO proposes the following formula to calculate the head-on collision force exerted by a vessel on a pier

$$P_S = 8.15 \times V\sqrt{DWT}, \quad (6)$$

where P_S is the equivalent static impact force of the ship (kip); DWT is the total displacement of the ship (tons); and V is the impact velocity of the ship (ft/s).

The horizontal length of the ship's bow deformed due to a collision with a rigid object is calculated as follows

$$a_s = 1.54 \times \left(\frac{KE}{P_s}\right), \quad (7)$$

where a_S is the length of bow damage (m); KE is the impact energy of the ship (J); and P_S is the impact force of the ship (N).

The average damage length of the ship's bow-a is calculated based on the average impact force applied to the working line-$P(a)$, such that

$$a = \frac{KE}{P(a)}. \quad (8)$$

AASHTO collects data from real-world accidents involving ships colliding with bridges, bridge piers, or other transportation structures. This data may include ship speed, size and weight of the vessel, time of collision, weather conditions, and the extent of damage to both the ship and the bridge. Fig.1 shows the typical collision force prediction based on two factors: vessel speed and displacement, according to statistical data.

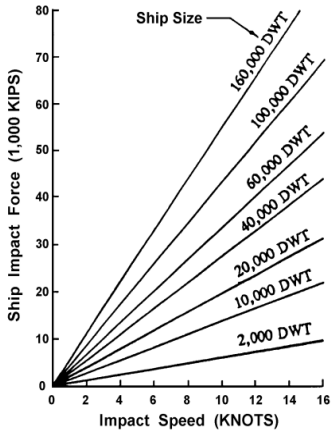

Figure 1. Typical collision force according to AASHTO [17]

1.5. Using numerical methods

The Finite Element Method (FEM) is extensively utilized in the simulation of structural collisions, including those involving bulbous bows. The bulbous bow, a protruding structure at the front of a ship, plays a critical role in hydrodynamics and structural integrity during collisions. FEM allows for detailed modeling and analysis of these collisions by discretizing the complex geometry of the bulbous bow and surrounding ship hull into finite elements.

In such simulations, FEM can capture the localized stress and strain distributions that occur upon impact. By applying FEM to model the dynamic interactions between the colliding vessels, researchers can assess the deformation, energy absorption, and potential damage to the bulbous bow. The method enables the evaluation of various collision scenarios under different conditions, providing valuable insights into the structural response and optimizing design features for enhanced collision resistance. FEM simulations help in predicting how the bulbous bow and hull structure will behave under impact, which is crucial for improving ship design and ensuring safety.

This application of FEM is instrumental in advancing the understanding of collision dynamics and developing more robust maritime structures that can better withstand the forces experienced during collisions.

1.6. Limitations

Although the ship's motion system during the collision has been expanded to 6 degrees of freedom (6DOF) to observe specific scenarios, the external dynamics of the impacted vessel, such as rolling and lateral movement, have not been analyzed in detail in this study. This omission may affect the model's accuracy in reflecting real-world phenomena in

complex environments. To improve this in future studies, integrating the analysis of forces and moments from water and surrounding conditions would enable more accurate simulations. Specifically, applying detailed hydrodynamic models and calculating uneven water flow around the ship could provide clearer insights into rolling and lateral movements during a collision.

The simulation of the bulbous bow focuses only on the main load-bearing structures, applying initial kinetic energy and a general material model for the entire structure. However, there has been no detailed consideration of internal structures such as beam configurations or reinforcement structures. A potential solution is to expand the model to include internal structures in more detail, by using finite element (FE) elements for beams and reinforcements. This would allow for a clearer assessment of the energy absorption capacity of these components during a collision.

The assumption that the rigid wall is absolutely inflexible to calculate maximum damage may lead to discrepancies compared to real-world conditions, where structures may exhibit a certain degree of elasticity. To address this issue, future studies could use nonlinear or semi-rigid material models, allowing rigid wall structures to display elasticity and absorb energy, thus better reflecting real-world scenarios.

Additionally, the rear structure of the ship has been simplified into a rigid beam, which, while saving computational resources, reduces the ability to fully assess the impact of collisions on these structures. To improve this, future research could expand the model to account for the effects of collisions on the entire vessel, including the rear structures. This could be achieved by using multi-scale finite element models, allowing for detailed focus in critical collision zones while maintaining simplicity in less significant areas.

2. Materials and Methods

2.1. Collision model

In order to save analysis time and optimize simulation performance in FEA explicit code, the selection of appropriate element types is crucial. In this study, two primary element types are employed: the Baelytschko-Tsay and Hughes-Liu elements, each with distinct characteristics and applications.

The Belytschko-Tsay element, a beam-shell type, is selected for the structural elements in the ship's bow, including frames, deck plates, and shell plating as depicted in Fig.2. This element uses a local coordinate system that deforms with the element, enabling more accurate simulation of deformations compared to standard shell elements while minimizing computation time. Specifically, the Belytschko-Tsay element supports single-point (reduced) and standard Gauss integration, with the reference plane set at the mid-surface. This configuration enhances simulation accuracy while maintaining computational efficiency.

The Hughes-Liu element is applied to the beam components of the ship's hull. This element is specifically designed to improve out-of-plane bending capabilities, which cannot be addressed by truss elements. This feature makes the Hughes-Liu element more suitable for modeling beam structures subject to bending and out-of-plane impacts that may occur during collisions, while also preventing fracture during the simulation process.

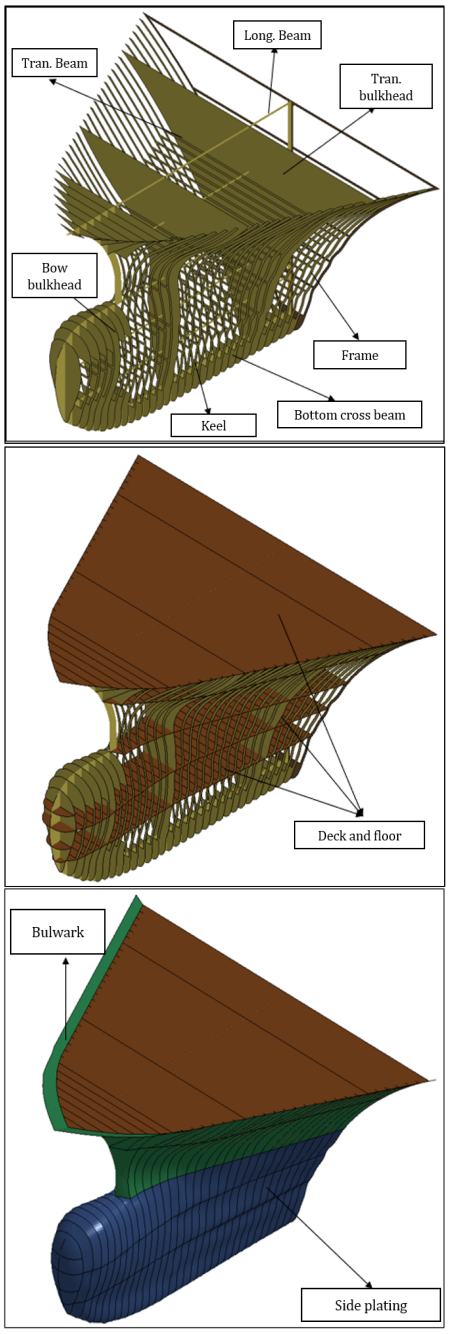

Figure 2. Construction of the bulbous bow structural model

The selection and application of these element types allow for accurate modeling of critical structural characteristics while optimizing computation time and resources in FEA explicit code.

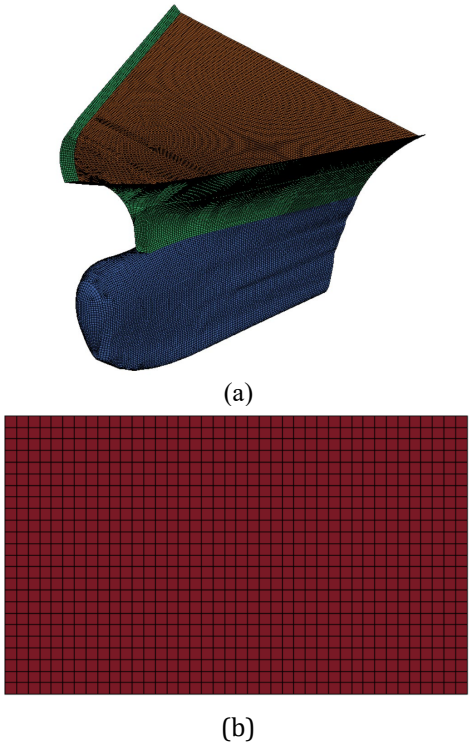

(a)

(b)

Figure 3. Mesh generation for the bulbous bow (a) and rigid plates (b)

In the process of collision simulation using FEA explicit code, mesh generation is a critical factor in achieving both accurate and efficient analysis results. Specifically, for the ship's pear-shaped bow and rigid wall models, appropriate meshing strategies must be applied to balance detail with computational performance. The ship's pear-shaped bow, playing a significant role in collision impact analysis, will be meshed with a very fine grid of 50×50mm as shown in Fig.3a. This allows for a detailed representation of geometric features and deformations in this critical region, thereby enhancing the accuracy of the analysis. Conversely, for the rigid wall structures, where there are no significant deformations and little influence on collision results, a coarser mesh of 500×500mm will be used as shown in Fig.3b. This approach is common in ship collision simulations as it simplifies computations, isolates the striking ship's response, and represents conservative estimates for design purposes.

2.2. Boundary conditions

Referencing the study by Yu and Amdahl [16], FEA is applied to simultaneously calculate both structural damage and the motion of the ship within a 6 DOF system. This approach is particularly useful for model design as it does not require detailed hull configuration. The user-defined load subroutine FEA provides nodal information such as displacement, velocity, acceleration, and user-defined inputs, allowing users to specify nodal loads or pressure loads as a function of this information. However, a challenge arises when applying added mass forces because nodal acceleration in the user-defined load subroutine is only available for deformable bodies and not for rigid bodies. If a deformable body is used to represent the ship's hull girder, it will generate significant structural vibrations, and the oscillation of nodal accelerations will yield inaccurate results.

Therefore, the hull girder is represented by a rigid beam [16], and the ship's COG velocity history is used to approximate the acceleration as follows

$$a_n = \frac{V_n - V_{n-2}}{t_n - t_{n-2}}, \tag{9}$$

where V_n and V_{n-2} are used instead of V_n and V_{n-1} because the code will otherwise yield numerical instabilities.

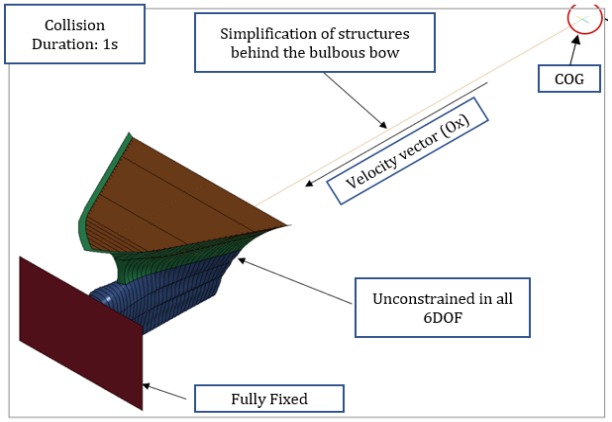

(a)

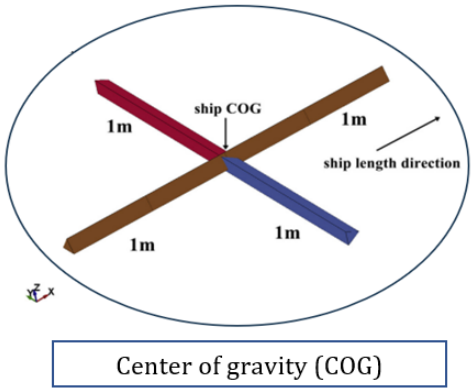

(b)

Figure 4. Setting up the collision model: (a) Overall collision and (b) ship COG

In Fig.4a, the ship's frame is represented by a long line extending from the bow to the center of gravity. Since the user-defined loading subroutine does not permit the application of bending moments, the user must convert these bending moments into force pairs. Consequently, several small beams.are created to facilitate the application of bending moments in roll, pitch, and yaw as performed in Fig.4b.

Two contact algorithms are employed: CONTACT_AUTOMATIC_SURFACE_TO_SURFACE and CONTACT_AUTOMATIC_SINGLE_SURFACE (ASTS &ASSC). The ASTS algorithm is selected for the contact between the bulbous bow and the rigid plate to prevent penetration between the meshes of differing sizes and material properties.

Given that the bulbous bow and the internal structure may undergo significant deformation during the collision, this could lead to interpenetration between elements. To mitigate this and improve simulation accuracy, the ASSC algorithm is applied with the same friction coefficient values as the ASTS algorithm. Although the use of ASSC increases computational time, it helps to adjust the contact points between the bulbous bow shell and the internal structure more realistically, accurately reflecting deformation in the simulation.

In this study, the static Coulomb friction coefficient is set to 0.5, and the dynamic Coulomb friction coefficient is set to 0.3. These values are chosen to accurately simulate the friction levels between contact surfaces under varying collision conditions. Karlsson [18] notes that a dynamic friction coefficient of 0.3 has been shown to be appropriate for collision simulations. To assess the impact of friction on the results, Odefey [19] conducted a series of simulations with dynamic friction values ranging from 0 to 0.3, demonstrating that the friction coefficient influences the differences in the increase of internal energy within the ship's structure, as well as the manifestation of various failure behaviors such as buckling, shearing and tearing.

2.3. Collision cases

The colliding ship is set to move at a constant velocity of 12 knots (~6.7 m/s) along the x-axis, with a weight of 330 DWT. Additionally, the ship's six degrees of freedom (6 DOF) are unconstrained to examine the actual movement of the ship post-collision. Besides the two factors directly affecting the initial collision kinetic energy, velocity and mass, this study will delve into the impact of collision position and angle.

Ofedey [19] studied the influence of collision angles on absorbed energy and deformation, revealing that collisions deviating by 15 degrees have a higher average absorbed energy compared to perpendicular collisions with the ship's hull. However, this may occur at larger deviation angles, as the bulbous bow may have the potential to slide backward and bounce off the attacked hull. To validate this assertion, the study will assess two collision angle scenarios as seen in Fig.5. perpendicular (90 degrees) and 45 degrees. External dynamics such as the inertia effects of surrounding water will be neglected to simplify the calculations; however, the post-collision movement of the impacted ship will be closely observed in 6 DOF.

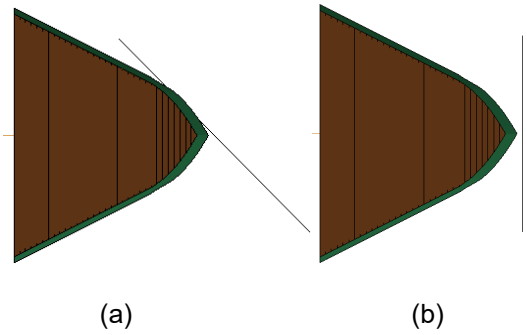

Figure 5. The collision angles tested in the report are 45 degrees (a) and 90 degrees (b)

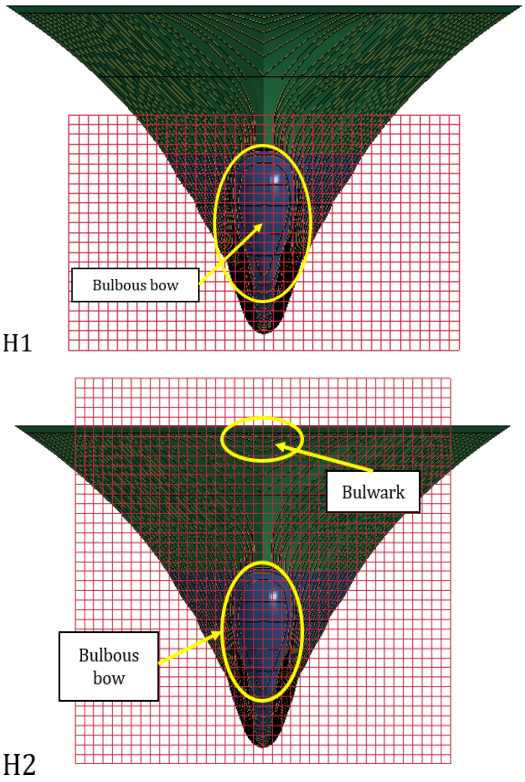

Figure 6. Two collision positions are tested in the report: H1-collision at the bulbous bow region and H2-collision of the bulbous bow and bulwark

In the study on collision damage conducted by Ozguc [20], an assessment was carried out for various collision positions. The results indicated that each collision position resulted in different amounts of absorbed energy and

distinct structural damage behaviors, suggesting that evaluating ollision positions is essential. In this study, two collision positions will be examined to assess their impact on energy absorption and the ship's post-collision movement (Fig.6).

2.4. Material model

The material is mild steel, and the material parameters applied are the results of standard tensile tests as shown and listed in Fig. 7 and Table1, respectively. From the study by Paik and Thayamballia [21], it was concluded that for simplified analytical analyses, the yield stress is approximately half of the sum of the yield stress and the ultimate tensile stress. This assumption has been shown to provide a good estimate in practice. Therefore, the static yield stress can be defined as

$$\sigma_0 = \frac{\sigma_y + \sigma_u}{2}, \quad (10)$$

where σ_y is yield stress; σ_u is ultimate strenght; σ_0 is static flow stress.

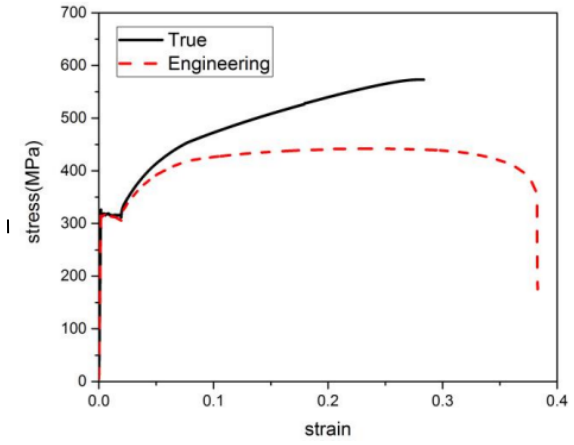

Figure 7. Stress-strain curve of the material tensile test [21]

The strain rate effect is considered in the dynamic crushing analysis below, and the Cowper-Symonds (1957) empirical formula is used to adjust the material parameters

$$\frac{\sigma_d}{\sigma_0} = 1 + \left(\frac{\varepsilon}{D}\right)^{1/q}, \quad (11)$$

where σ_s is the static flow stress; σ_d is the dynamic flow stress; and ε is the strain rate.

Model 024_PIECEWISE_LINEAR_PLASTIC is used to describe lightweight steel for the entire bow structure. This material type allows for the simulation of strain rate effects and complete material failure under severe impact conditions. The material behavior is characterized by parameters such as Young's modulus, yield stress, shear modulus, damage strain, and Cowper-Symonds strain rate parameters. These parameters enable the lightweight steel to accurately respond to dynamic impacts and large deformations.

The material model 020_RIGID is applied to the ship's central beam and rigid wall structures. The 020-material type is commonly used in models requiring the specification of absolutely rigid elements. These rigid elements are unaffected by deformation processes, significantly reducing computation time in complex simulations. By neglecting their deformation, computational resources are optimized while maintaining the accuracy of the results. Table 1 provides comparative properties for mild steel, HT32, and HT36, but only mild steel was used in FEM simulation due to its common use in ship hulls for ductility and cost-effectiveness. It is worth noting here that higher grades HT32 and HT36 have increased yield stress (315-355 MPa vs. 235 MPa) and ultimate tensile stress (530-560 MPa vs. 450 MPa), but lower critical failure strain (16.5-15% vs. 20%), leading to reduced deformation (less indentation) but potentially higher peak forces and altered failure modes (e.g., earlier fracture). In ship bow collisions, this can enhance energy absorption capacity in some cases, as higher-strength steels resist buckling and tearing better, reducing overall damage area.

Table 1. Material properties to be used in nonlinear FE analyses [20]

Material properties	Steel grade		
	Mild	HT32	HT36
Yield stress (MPa)	235	315	355
Elastic strain (%)	0.20	0.20	0.20
Ultimate tensile stress (MPa)	450	530	560
Critical failure strain (%)	20.0	16.5	15.0
Density (kg/mg3)	7850	7850	7850
Young's modulus (GPa)	206	206	206
Poisson's ratio	0.3	0.3	0.3
Tangent modulus (MPa)	1085	1303	1385
Hardening parameter	1.0	1.0	1.0
Strain rate (C)	40.4	3200	3200
Strain rate (P)	5.0	5.0	5.0

3. Results and Discussion

3.1. Verify simulation results

AASHTO formulas are used for a range of vessel displacements and velocities. In this report, to verify the accuracy of the pear-shaped bow damage collision model, the simulation results will be compared with the theoretical calculation formulas provided in the AASHTO guidelines presented in [17].

Table 2. Conformity of the calculated parameters vessel sizes analyzed in this study with AASHTO recommendation [17]

Parameters	Current work	AASHTO [17]
Impact velocity (knots)	12	0-16
Impact mass of the ship (DWT)	330	0-160000

Table 3 compares the collision force and indentation of the report model with AASHTO. The results from the simulation in this current work show that the maximum collision force of the report model deviates from the theoretical formula by approximately 25%, and the collision indentation shows a deviation of 26%. The discrepancies in force and indentation may be attributed to the effects of shell thickness and internal structures. Therefore, the model in the report is considered suitable according to AASHTO for proceeding with the subsequent evaluation steps.

Table 3. Comparison of the collision force and indentation of the current work with AASHTO [17]

Parameters	Current work	AASHTO [17]	Differences (%)
Impact Force (MN)	17,600	13,204	25
Deformation (m)	0,766	0,566	26

3.1. Absorbed energy

Regarding energy absorption, in practice, besides the bulbous bow structure, the collision object (a rigid wall), as well as factors such as impact cushioning and the surrounding water environment, also contribute to the absorption of collision energy. However, in this simulation report, the collision object is considered to be absolutely rigid, and the other factors are neglected. Thus, it is assumed that the collision energy is entirely absorbed by the ship's bow structures through the deformation of the shell plating and internal structures. Therefore, the total energy absorbed by the ship's bow [22] in the collision is calculated using the formula

$$EA = \int P(\delta) d\delta \,. \qquad (12)$$

By combining Eq.11 and Eq.12, the total energy absorbed by the bulbous bow (EA) is equivalent to the area under the force-displacement curve [22]. Therefore, EA can be calculated using the following formula

$$EA = \sum_{i=1}^{n} (P_i + P_{i+1}) \times \left(\frac{\delta_{i+1} - \delta_i}{2}\right), \qquad (13)$$

where P_i and δ_i are the ith impact force and instantaneous indentation, respectively, among the n results.

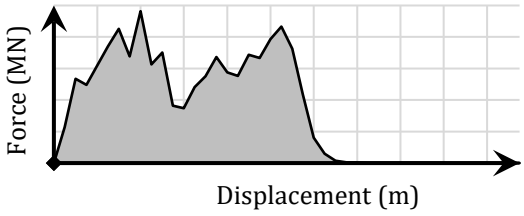

Figure 8. Force-displacement curve of the bulbous bow structure collision simulation

3.2. Effect of the collision angle

Typically, a perpendicular collision results in the highest impact force and damage indentation. However, collisions at different angles are also an important factor to consider carefully, as they affect the structural response to deformation forces and the impact of the angle on post-collision energy, which will be discussed later.

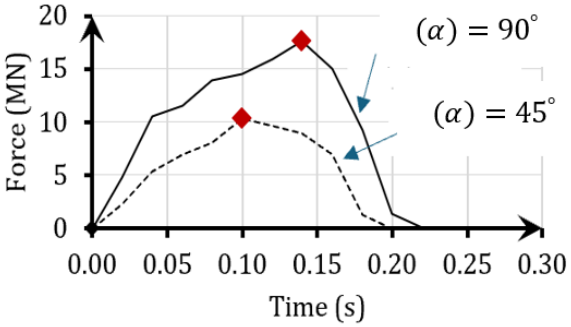

Figure 9. Force-time curve for two FEM collision angles

In Fig.9, when the collision angle (α) changes from 90 degrees to 45 degrees, the impact force decreases immediately by 41.1% from 17.6 MN to 10.37 MN. In the theoretical formula provided by AASHTO for calculating impact force, the effect of the collision angle is not considered, so the results from the simulation cannot be compared with the theoretical formula.

As seen in Fig.10, the collision indentation in the model at $(\alpha) = 45^{\circ}$ is 1.62 times greater than at $(\alpha) = 90^{\circ}$ (0.915 m compared to 0.566 m). This is because, when colliding at an oblique angle, the contact area is reduced, which means that fewer shell plating and internal structures are

engaged to resist the external impact force, resulting in greater indentation of the bulbous bow, as illustrated in Fig.11. The collision angle does not affect the formula for calculating the initial kinetic energy of the collision, so both models at $(\alpha) = 45^{\circ}$ and $(\alpha) = 90^{\circ}$ have the same initial kinetic energy value, KE_initial (6.41 MJ).

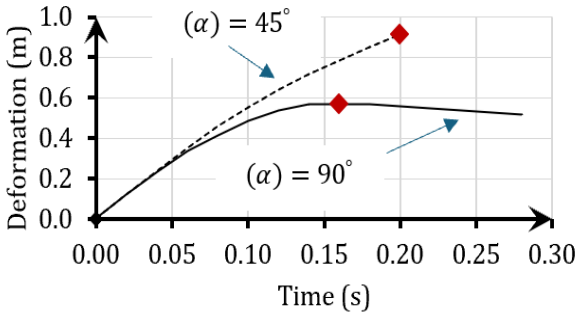

Figure 10. Deformation-time curve for two FEM collision angles

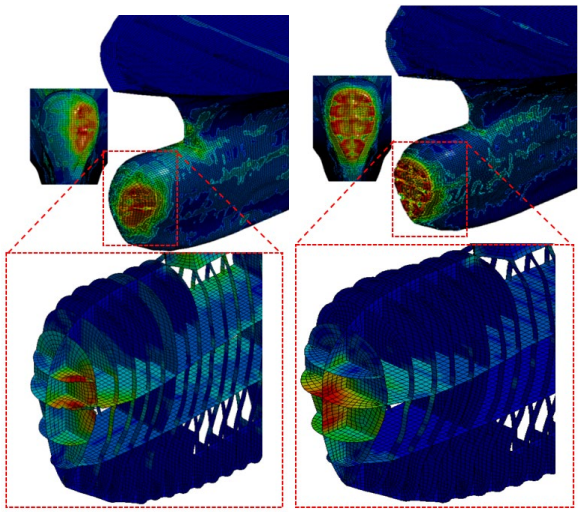

Figure 11. Damage to the internal structure of the bulbous bow in two collision angle models: (a) $(\alpha) = 45^{\circ}$ and (b) $(\alpha) = 90^{\circ}$

Examining the kinetic energy results at the end of the collision, differences between the models are evident. The model at $(\alpha) = 45^{\circ}$ results in post-collision kinetic energy of 3.7% (0.24 MJ compared to 6.41 MJ), while the model at $(\alpha) = 90^{\circ}$ shows a post-collision kinetic energy of 52.57% (3.37 MJ compared to 6.41 MJ) of the initial kinetic energy. Additionally, the post-collision kinetic energy of $(\alpha) = 45^{\circ}$ is 14 times greater than that of the $(\alpha) = 90^{\circ}$ model (3.37 MJ compared to 0.24 MJ), indicating that the collision angle significantly affects the transformation and absorption of kinetic energy in the analyzed model.

From Fig.12, an analysis of the calculated absorbed energy (EA) and internal energy output from FEA (IE) shows that for the model with $(\alpha) = 45^{\circ}$, there is a discrepancy of 66.5% between the two values, while the model with an angle of $(\alpha) = 90^{\circ}$ shows a discrepancy of 6.8%.

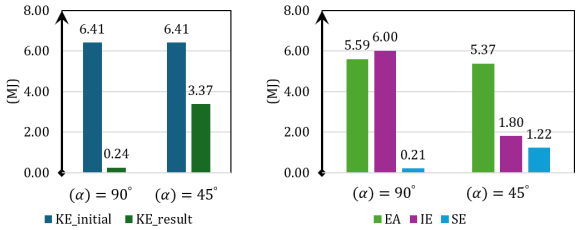

Figure 12. Energy analysis results under the influence of collision angle

It is observed that changing the collision angle significantly alters the internal energy value post-collision for the two models (1.80 MJ versus 6.00 MJ). To explain the large discrepancy between internal energy and absorbed energy, it is possible that the internal energy values integrated in FEA explicit code account only for energy-absorbing structures and do not consider external dynamic energy. For the surface shear energy (SE) results, the $(\alpha) = 45^{\circ}$ angle case yields result approximately 6 times greater than the $(\alpha) = 90^{\circ}$ angle model (1.22 MJ versus 0.21 MJ). This indicates that the collision angle has a significant impact on the shear energy of the analyzed model.

The absorbed energy (EA) for the cases with $(\alpha) = 45^{\circ}$ and $(\alpha) = 90^{\circ}$ does not show a significant difference (5.59 MJ versus 5.37 MJ). This suggests that the observation by Ofedey [16] that impact angles deviating from a perpendicular $(\alpha) = 15^{\circ}$ or more tend to decrease absorbed energy is substantiated. In the case of $(\alpha) = 45^{\circ}$, the impact force is only 58.9% of that at $(\alpha) = 90^{\circ}$; however, it results in a deformation that is 1.62 times greater, leading to minimal differences in absorbed energy. This indicates that Minorsky's method does not account for the coverage distance when impacts occur from different angles. This also aligns with the statement by Pedersen and Zhang [23] that Minorsky's method overlooks structural arrangement, material properties, and damage modes.

3.3. Impact of the Collision Location Factor

The simulation results show that model $H2$ experiences the collision 0.06 seconds earlier than model $H1$ (0.08 seconds versus 0.14 seconds) because the bow section of the wave shield collides with the rigid wall first. Observing Fig.13, although there is a difference in the collision initiation time

between the two models, the results for the maximum collision force are similar, with a discrepancy of only 3.8% (17.6 MN versus 18.295 MN), and both models reach their peak force at the same time, 0.28 seconds. It can be concluded that, within the scope of this study, the two collision locations under consideration do not yield significant differences in the collision force values.

The post-collision deformation of model $H1$ is only 62.2% of that of model $H2$ depicted in Fig 14, although both models achieve their maximum deformation at the same time (0.3 seconds). This indicates that, despite model $H2$ absorbing part of the collision force through the wave

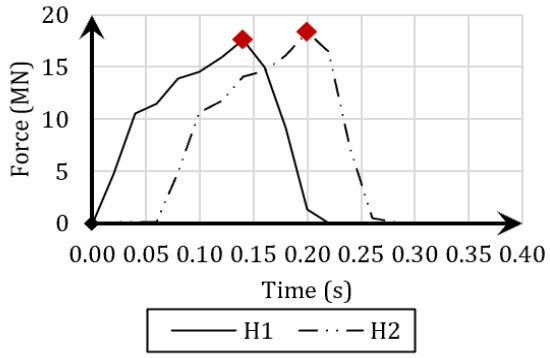

Figure 13. Force-Time Curve for collision at two test collision locations

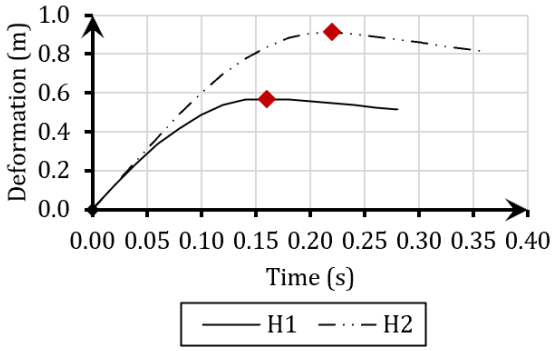

Figure 14. Deformation-Time Curve for collision at two test collision locations

shield structure, the deformation observed is still greater compared to the case of a single collision at the bulbous bow structure. This can be explained by the fact that the deformation in case $H2$ accounts for damage to the edge structure as well, and the resistance of this structure to the impact is relatively low as seen in Fig 15. Similar to the collision angle, the collision location does not affect the formula for calculating the initial collision kinetic energy, so both models $H1$ and $H2$ have the same initial kinetic energy value (6.41 MJ).

The results for post-collision kinetic energy show that model $H1$ has 3.7% of the initial collision energy (0.24 MJ compared to 6.41 MJ), while model $H2$ has 2.5% (0.16 MJ compared to 6.41 MJ), with a discrepancy of approximately 33.34% (0.16 MJ compared to 0.24 MJ)

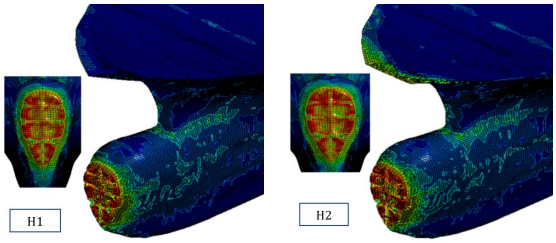

Figure 15. Collision simulation of the internal structure of the bulbous bow at two collision locations

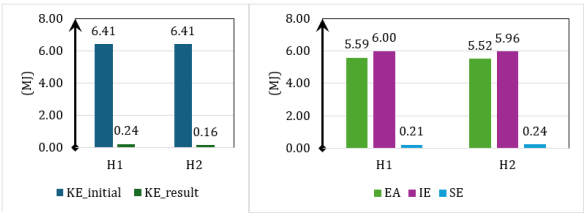

Figure 16. Energy analysis results under the influence of collision position

between the two models. This indicates that both collision locations in the models convert and absorb nearly all of the initial kinetic energy, with minimal differences in the post-collision kinetic energy results. This can be explained by the fact that in model $H2$, the kinetic energy is absorbed by two structural components: the wave shield and the bulbous bow, resulting in a discrepancy in the post-collision kinetic energy of the bulbous bow due to the prior absorption by the wave shield.

Similarly to the kinetic energy analysis, the post-collision energy values for the models show minimal variation across different collision locations. Specifically, model $H1$ exhibits discrepancies of 1.3% in absorbed energy (5.52 MJ compared to 5.59 MJ), 0.01% in internal energy (5.96 MJ compared to 6 MJ), and 12.5% in surface shear energy (0.24 MJ compared to 0.21 MJ) compared to model $H2$. It can be concluded that the energy values for both models, before and after the collision, are not significantly affected by the collision location used in the analysis. However, it is anticipated that for cases with higher input kinetic energy, different collision locations may yield more varying results.

3.4. Post-collision ship motion

Both models with angles $(\alpha) = 45^{\circ}$ and $(\alpha) = 90^{\circ}$ were tested at a speed of 12 knots. However, the simulation results show that the collision in the $(\alpha) = 45^{\circ}$ model occurs earlier than in the $(\alpha) = 90^{\circ}$ model (0.04 seconds versus 0.14 seconds), but the collision duration is shorter (0.2 seconds versus 0.28 seconds). To explain this, Fig.17 shows that in the $(\alpha) = 45^{\circ}$ model, during the collision (from t = 0 to t = 1), the ship's centerline tends to rotate and gradually slide parallel to the surface of the rigid wall, leading to a significant reduction in both collision force and duration. This occurs because at larger angles, the bulbous bow, when colliding with the rigid wall, tends to rebound due to the ship's inertia, impact reaction forces, and other external dynamic effects.

Considering external dynamic models along with internal mechanical damage always yields the most detailed and realistic results. However, depending on the specific research case, flexibility in applying the analytical method can be exercised. To demonstrates scalability, as

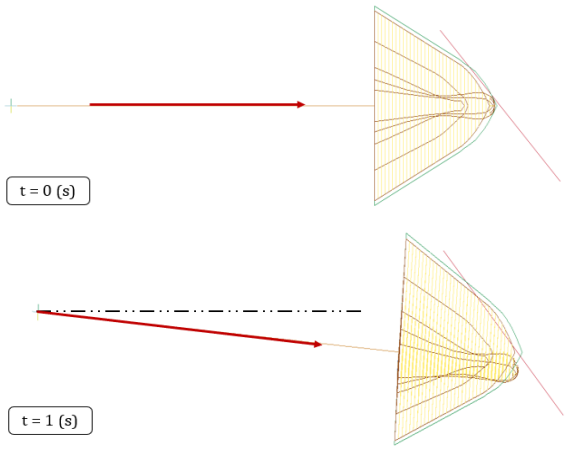

Figure 17. Ship motion before and after collision in the case of $(\alpha) = 45^{\circ}$ collision angle

larger masses lead to proportionally higher impact forces and absorbed energy, for instance, in the model shown in Fig.18, the bulbous bow collides perpendicularly with a rigid wall at a speed of 12 knots and a mass of 2073 DWT (instead of 330 DWT). With a direct collision angle and high initial kinetic energy, the resulting collision force, indentation, and absorbed energy are significant. In this case, external dynamic modeling, energy dissipation, and rotational movements can be excluded to conserve computational resources. The decoupling method from external dynamics simplifies the fluid effects as a constant added mass and applies the conservation of momentum principle, providing a quick and reasonable estimate of energy dissipation and structural damage.

4. Conclusions

The values for impact velocity and vessel mass in this study have been referenced from statistical data ranges provided by AASHTO related to actual collision incidents. Verification of the simulation was conducted by comparing FEM results with those obtained from the theoretical formulas of AASHTO. The maximum collision force of the report model deviates from the theoretical formula by approximately 25%, and the collision indentation shows a deviation of 26%. The discrepancies in force and indentation may be attributed to the effects of shell thickness and internal structures. The model in the report is considered suitable according to AASHTO for proceeding with the subsequent analysis steps.

Similar to the factors directly influencing the initial kinetic energy, such as velocity and mass, collision angle (α) and impact location (H) are also important factors affecting the absorption of collision forces by the hull and internal structures. Moreover, these two factors are crucial when considering external dynamic models, energy dissipation through fluids, and rotational movements.

In this study, the results show that at $(\alpha) = 45^{\circ}$ collision angle, there is a significant reduction in collision force. However, the indentation is greater, leading to minimal differences in energy absorption compared to a perpendicular collision angle. Nevertheless, the energy associated with sliding shows a considerable increase, and post-collision movement effects should also be considered. This indicates that incorporating external dynamic models, such as the effects of water, rotational movements, and swaying, is essential for accurate collision analysis.

Impact location cases were also examined in the study, but the results revealed no significant differences between the two cases. However, it is anticipated that in simulations with higher initial kinetic energy, the influence of impact location on energy absorption would become more pronounced.

Minorsky's theoretical formula relies solely on initial kinetic energy to determine collision force and indentation, which essentially converts kinetic energy into force and indentation values. However, real-world collisions are far more complex, with force and indentation fluctuating over time. Therefore, the formula's results should be viewed as preliminary estimates.

An analysis of the ship's motion indicates that external dynamic models significantly impact energy absorption in collisions. Optimal research on complex collisions requires a combined approach, utilizing both internal mechanics and external dynamics. However, there must be flexibility, as simplified, decoupled methods can still be applied in cases where external dynamic effects are negligible, helping to conserve computational resources. For future work, suggestions can be proposed by incorporating deformable models for the struck structure (e.g., nonlinear materials) to better capture mutual deformation, as recommended in the literature.

Acknowledgements

We acknowledge the support of time and facility from Ho Chi Minh City University of Technology (HCMUT) and Vietnam National University-Ho Chi Minh City (VNU-HCM) for this study.

References

[1] Yu Z, Shen Y, Amdahl J, Greco M. Implementation of Linear Potential-Flow Theory in the 6DOF Coupled Simulation of Ship Collision and Grounding Accidents. J Ship Res. 2016;60(3):114–119.
[2] Hong L, Amdahl J. Rapid assessment of ship grounding over large contact surfaces. Ships Offshore Struct. 2012;7(1):5–19.
[3] Simonsen BC. Ship grounding on rock—I. Theory. Mar Struct. 1997;10(7):519–562.
[4] Yu Z, Hu Z, Wang G. Plastic mechanism analysis of structural performances for stiffeners on bottom longitudinal web girders during a shoal grounding accident. Mar Struct. 2015;40:134–158.
[5] Pan J, Wang T, Zhang WZ, Huang SW, Xu MC. Study on the assessment of axial crushing force of bulbous bow for bridge against ship collision. Ocean Eng. 2022;255:111411.
[6] Wang Z, Guo C, Wang C, Chen G, Xu Y, Li Q. An analytical method for predicting the structural response of ship side structures by bulbous bow in oblique collision scenarios. Ships Offshore Struct. 2023;19(10):1490–1503.
[7] Liu B, Villavicencio R, Pedersen PT, Guedes Soares C. Analysis of structural crashworthiness of double-hull ships in collision and grounding. Mar Struct. 2021;76:102898.
[8] Minorsky V. An analysis of ship collisions with reference to protection of nuclear power plants. New York: Sharp (George G.) Inc; 1958.
[9] Reardon P, Sprung JL. Validation of Minorsky's Ship Collision Model and Use of the Model to Estimate the Probability of Damaging a Radioactive Material Transportation Cask During a Ship Collision. In: Proceedings of the International Conference on Design and Methodologies for Collision and Grounding Protection of Ships; August 1996; San Francisco. 1996.
[10] Paik JK, Chung JY, Choe IH, Thayamballi AK, Pedersen PT. On the Rational Design of Double Hull Tanker Structures Against Collision. HHI Eng Rev. 2005;25(3):41–51.
[11] Pedersen PT, Zhang S. On Impact mechanics in ship collisions. Mar Struct. 1998;11(10):429–449.
[12] Stronge WJ. Impact Mechanics. Cambridge, UK: Cambridge University Press; 2004.
[13] Yu Z, Amdahl J. Influence of 6DOF ship motions in the damage prediction of ship collision and grounding accidents. In: Proceedings of the 7th International Conference on Collision and Grounding of Ships and Offshore Structures; June 15–18, 2016; Ulsan, South Korea. ResearchGate; 2016.
[14] Motora S, Fujino M, Sugiura M, Sugita M. Equivalent Added Mass of Ship in the Collision. J Soc Naval Archit Jpn. 1969;126:141–152.
[15] Tabri K. Influence of coupling in the prediction of ship collision damage. Ships Offshore Struct. 2012;7(1):47–54.
[16] Yu Z, Amdahl J. Full six degrees of freedom coupled dynamic simulation of ship collision and grounding accidents. Mar Struct. 2016;47:1–22.
[17] American Association of State Highway and Transportation Officials (AASHTO). Guide specification and commentary for vessel collision design of highway bridges. Volume I, final report. Washington DC: AASHTO; 1991.
[18] Karlsson UB. Improved Collision Safety of Ships by an Intrusion-Tolerant Inner Side Shell. Mar Technol SNAME News. 2009;46(3):165–173.
[19] Odefey M. Simulation of Collisions between RORO Vessels with Improved Double-Hull Designs – Influence of Modelling Parameters in Explicit Finite Element Analysis. [Master's thesis]. Gothenburg (Sweden): Chalmers University of Technology; 2011. 146 p.
[20] Ozguc O. Structural damage of ship–FPSO collisions. J Mar Eng Technol. 2017;18(1):1–35.
[21] Paik JK. Ultimate Limit State Analysis and Design of Plated Structures. London: Wiley; 2018.
[22] Yuan P, Harik IE. One-Dimensional Model for Multi-Barge Flotillas Impacting Bridge Piers. Comput-Aided Civ Infrastruct Eng. 2008;23(6):437–447.
[23] Chen J, Zhu L, Pedersen PT. On Dynamic effects of Bulbous Bow Crushing. In: Proceedings of the 29th International Ocean and Polar Engineering Conference; 2019; Honolulu, Hawaii. Cupertino, CA: International Society of Offshore & Polar Engineers; 2019. p. 4288–4295.